Spectrum of Engineering Sciences
ISSN (e) 3007-3138 (p) 3007-312X Volume 4, Issue 3, 2026

ION HEIGHT TRADE-OFF WITH PSEUDOPOTENTIAL STRENGTH: IMPLICATIONS FOR MOTIONAL HEATING, OPTICAL ACCESS, AND SCALABILITY IN LARGE-SCALE ION-TRAP ARRAYS

*[1]**Kaz Bano**

*[1]*Ph.D. Scholar, Institute of Physics, University of Sindh, Jamshoro.*
*[1]kazbano@scholars.usindh.edu.pk

Keywords
ion trap, pseudopotential, motional heating, anomalous heating, quantum computing, surface-electrode trap, optical access, quantum charge-coupled device

Article History
Received on 14 Feb, 2026
Accepted on 20 Feb, 2026
Published on 29 March, 2026

Copyright @Author
Corresponding Author:
Kaz Bano

Abstract

Scaling surface-electrode ion traps to hundreds of qubits requires a careful balance between competing geometric constraints. Reducing the ion height above the electrode plane deepens the radiofrequency pseudopotential and stiffens confinement, yet it simultaneously enhances anomalous motional heating and restricts the numerical aperture available for laser addressing and fluorescence collection. This study quantifies these trade-offs across an ion-height range of 30 to 200 micrometres using a simulated dataset of 18 configurations and ten derived performance metrics. Power-law, exponential, and polynomial regression models were applied to characterize heating-rate scaling, pseudopotential decay, and array performance. The motional heating rate followed an inverse power-law in ion height with exponent $\alpha = 2.02$ *(nonlinear least-squares fit,* $R^2 = 0.988$*), while the pseudopotential depth decayed exponentially with a decay constant of* $0.0269\ \mu m^{-1}$ *(*$R^2 = 0.990$*). A composite figure of merit combining trap stability, gate fidelity, optical access, and array capacity peaked at 132 μm (FOM = 0.969,* $R^2 = 0.999$*), identifying this height as the optimal design point for balancing trapping strength against decoherence. Pearson correlation analysis revealed near-perfect positive coupling between ion height and trap stability (*$r = 1.00$*) and near-perfect negative coupling with radial secular frequency (*$r = -0.95$*). These results provide quantitative design guidance for next-generation quantum charge-coupled device architectures and support the growing consensus that mid-range ion heights offer the most favourable operating regime for scalable trapped-ion quantum computing.*

Introduction

Radiofrequency (RF) Paul traps, which confine atomic ions trapped within the Paul trap, are still one of the most developed and highest-performing physical systems to implement quantum information processing, with long coherence times, near-perfect state preparation and readout and two-qubit gate fidelities that regularly exceed 99.9 percent in state-of-the-art laboratories (Löschnauer et al., 2 With commercially available devices like IonQ and Quantinuum joining academic consortia in the move to the quantum charge-coupled device (QCCD) architecture, as the field transitions to noisy intermediate-scale quantum (NISQ) demonstrations and next to fault-tolerant logical qubits, the quantum charge-coupled device (QCCD) architecture has become the most promising scaling route beyond the constraints of a single, monol The QCCD paradigm spatial arrangement encompasses tens to hundreds of ions per networked, microfabricated surface-electrode traps with ion shuttling, interaction, storage and readout taking place in special functional regions. This architectural transition has generated a design challenge by the side: all geometric and electrical parameters of the surface trap now have a tradeoff with a variety of competing performance measures and there is no single configuration that provides optimal performance on all measures simultaneously.

One of these parameters is the height h of the ion above the electrode plane which takes a rather central position. The height also determines (a) the depth and curvature of the RF pseudopotential confining the ion, (b) the rate of anomalous motional heating of the ion by the fluctuating electric fields on the surface of the surrounding electrode, (c) the solid angle that the laser can access and the fluorescence can be observed, (d) the susceptibility of the ion to excess micromotion by stray DC fields, and These are not weak and benign dependencies. Pseudopotential depth scales to the order of exponentially in h, and heating rates in the canonical fluctuating-patch model scale to the inverse fourth power of the distance between ions and electrode, which has been experimentally validated in a variety of different platforms (Brownnutt et al., 2015; Sedlacek et al., 2018). The result is that low ion heights lead to tight confinement, high secular frequencies, and rapid gates at the price of catastrophic motional heating; and high ion heights at the price of impractical RF voltages to stabilize and ensure the array density which can be obtained on a given footprint.

Although this trade-off lies at the centre, quantitative and integrated design advice exists in sub-disciplines. Experimental works typically have scaled heating-rate with single trap geometry (An et al., 2019; Sedlacek et al., 2018), theoretical work has focused on individual noise-generation mechanisms (Safavi-Naini et al., 2011) and engineering work has typically assumed that trap height is an input parameter to be optimized rather than a design parameter. The current work fills this gap by mapping the height-dependent behaviour of eight coupled performance metrics in a physically realistic range (30 to 200 μm) and fitting each of the metrics to the best parametric model, then integrating them into a composite figure of merit (FOM) which can be maximized to determine an optimum operating point.

The analysis is guided by three main research questions. First, to what extent can such simple parametric models as inverse power laws to heating, exponential decay to pseudopotential depth, and linear scaling to secular frequencies on log scales, be used to describe the coupled behaviour of the trap parameters over a two-order-of-magnitude range of ion height? Second, at what operating height will a composite figure of merit that trades between gate fidelity, trap stability, optical access and array scalability be optimized? Third, what pairs of performance metrics are the most strongly coupled, and which may be optimized separately, with the help of auxiliary methods, like surface treatment, integrated photonics, or cryogenic operation? The answers to these questions are practical advice to trap designers and give perspective on the limits of the design space that the design will have to operate within in the future, by scalable ion-trap quantum processors.

The rest of this paper will be structured in the following way. The literature review places the current work in the context of 20 years of experimental and theoretical studies on anomalous heating and the design of surface traps. The methods section explains the dataset, the parametric models that were used and the statistical procedures that were used to estimate the regression coefficients and regression coefficient uncertainties. The results section shows the fitted models, the correlation structure between the trap parameters as well as the optimization of the composite figure of merit. These findings are discussed in the context of the present-day QCCD roadmaps and the conclusion summarizes the implications on the design of the next-generation large-scale ion-trap quantum processors.

Literature Review

Radiofrequency Paul traps and Pseudopotential Approximation

To confine charged particles by time-varying electric fields in a Paul trap is traditionally discussed within the framework of the pseudopotential approximation, which substitutes the fast-varying RF field, with an effective time-independent ponderomotive potential well (Berkeland et al., 1998). With the surface-electrode linear trap, the pseudopotential depth at the trap centre is approximately proportional to (q e V 0) 2 / (4 m O 2 h 2) h being the ion height above the electrode plane, m the ion mass and q the resultant Mathieu q-parameter (Chiaverini et al., 2005; Wineland et al., 1998). This inverse square dependence on confinement depth and ion height is in practice controlled by the finite size of the RF electrodes, so that it is usually more steeply decreasing with h as in the case of realistic planar geometries (Abbasov et al., 2023). This means that to get a trap depth large enough to enable vigorous loading and extended operation times (generally 0.05 eV or larger) is either low ion height, or very high RF voltages, which cause penalties elsewhere in the design space.

The axial and radial secular frequencies, ωz and omega r, respectively, are a measure of the harmonic confinement stiffness and determine the rate of the natural clock of the motional-mode-based entangling gates. These frequencies are proportional to the inverse of h, by the dependence on the curvature of the pseudopotential at the trap minimum. The increased frequencies of the secular currents allow higher rates of gates and greater protection against low-frequency noise in the electric field but require equally higher values of Mathieu q-values, which also can push the trap to the edge of dynamical stability (Berkeland et al., 1998; Home, 2013). In well-designed linear traps, the secular-frequency ratio ωr/2 omega z is usually restricted to a range of 1.73 to 1.82, to make sure that radial modes are uniformly resolvable through the ion string, without overlapping with the axial modes.

Abnormal Motional Noise of Heating and Electric-Field

The observation of anomalous motional heating, i.e. the fact that trapped ions become heated many times faster than it should due to Johnson-Nyquist thermal noise by resistivity of conductors, has been a long-standing impediment to scaling trapped-ion systems over the past 20-plus years (Brownnutt et al., 2015; Turchette et al., 2000). Empirical measurements of the motional heating rate ṅ with ion-electrode distance d over a broad variety of experimental platforms have been found to follow a power law ṅ ∝ d - (a range of) 2-4, depending on the noise mechanism of interest and the surface conditions (Deslauriers et al., 2006; Sedlacek et al., 2018). An exponent of 4 is predicted by the canonical fluctuating-patch model, where independent microscopic dipoles on a conductor surface cause uncorrelated potentials, to predict an exponent of 4 in point-like ions suspended far above a planar electrode (Low et al., 2011). Exponent values measured in needle traps and multi-zone surface traps have been found to cluster around this value, with Deslauriers et al. (2006) and Sedlacek et al. (2018) observing a d^(−4) scaling in five discrete ion heights in room-temperature and cryogenic operation, respectively. The cause of this noise at the microscopic level is not fully comprehended. Two-level fluctuators due to adsorbed contaminants, patch-potential variations caused by polycrystalline grain boundaries and dielectric loss due to exposed insulating surfaces are all candidate mechanisms (Hite et al., 2021; Safavi-Naini et al., 2011). Great advances have been achieved in the damping of the noise by surface treatments: in situ argon-ion milling has shown to reduce heating by a factor of up to a hundred (Hite et al., 2012), and cryogenic operation has shown to reduce heating by a factor of one to two (Sedlacek et al., 2018). However, the heating rates of a few thousand quanta per second per mode at ion heights below 50 m are still characteristic of the state-of-the-art treated surfaces, and such tight traps are not a good choice in high-fidelity quantum logic without strong countermeasures.

Access, Addressing and Photonics Photonics Optical Access, Addressing, and Integrated Photonics.

Addressing ions using laser beams which are tightly focused and collection of resonance fluorescence are all geometrically limited due to ion height. The higher the ion position, the larger the numerical aperture (NA) to collection and addressing optics, and the half-angle of unobstructed optical access is approximated to follow arctan(h/Delta), where Delta is the lateral dimension of blocking structures like wire bonds or neighbouring electrodes (Abbasov et al., 2023). Quantum computers based on ion trap should have scales large enough to need beam waists on the order of a few micrometres, which in turn implies that there is a need to have an effective NA of 0.35-0.5mm- effective- NA- something which is difficult to achieve at ion heights smaller than around 50 mm without compromising the integrity of the electrode plane (Malinowski et al., 202

More recent developments in integrated photonics have already started to loosen these limitations by providing addressing and cooling of light using on-chip waveguides and grating couplers, instead of bulk free-space optics. Mordini et al. (2025) demonstrated in a surface trap with integrated photonic delivery the first multi-zone coherent operations, demonstrating Ramsey sequences in two trapping zones (separated by 375 μm) and light delivered through grating couplers under the ion. Kwon et al. (2024) applied this method to the concurrent control of several ^{171}Yb + ions with multi-mode interferometer splitters, providing all the wavelengths to control the qubit. These combined methods however still require having an ion height large enough to prevent stray-field heating of bare dielectric surfaces and to achieve the desired waveguide-to-ion vertical separation.

The Quantum Charge-Coupled Device Architecture Scaling

QCCD architecture It was introduced by Kielpinski et al. (2002) to divide trapped ions into memory, interaction, loading, and detection regions linked together with junction regions that an ion is shuttled between with time-varying DC potentials. Modern realizations by Quantinuum and partners have achieved up to 56 real physical qubits running with a quantum volume of more than two million on the H2 system (Moses et al., 2023), and commercial directions have hundreds of physical qubits by 2027 with a clear roadmap to fault-tolerant logical qubits based on surface codes (Chen et al., 2024; Litinski et Scalability experiments by Malinowski et al. (2023) and architectural investigations by Litinski et al. (2025) have found shuttling speed, heating of junctions, and solution to fidelity to be the key limiting factors to further expansion-all of which are highly coupled to the ion-height parameter of interest here.

The second body of work has been on alternative trap topologies which decouple some of these competing constraints. Jain et al. (2024) fully quantum-controlled a single ^{9}Be+ ion in a microfabricated Penning trap; RF field was replaced by a 3 T magnetic field, and heating due to pseudopotential was completely eliminated, but at the cost of an much more complex cryogenic and magnetic-shielding infrastructure. Skeleton electrodes printed in three dimensions with improvements of over 50% in heating by reducing the area around the electrode have also been theorized (Reens et al., 2024), but have yet to be demonstrated experimentally. These alternative methods are valuable compliments to, and not substitutes of the surface-electrode RF trap that has crushing advantages in manufacturability, compatibility with microfabrication, and with planar photonics.

Research Gap

Despite the well-known individual height-dependent scaling laws of heating, confinement, and optical access, relatively little has been done, to date, to optimize them with a single composite figure of merit. Current literature (Brown et al., 2021; Brownnutt et al., 2015) has thoroughly treated the subject of electric-field noise but has not gone as far as to discuss the array-level performance metrics of gate fidelity, crosstalk and addressing efficiency. Architectural explorations (Malinowski et al., 2023) on the other hand consider parameterized fixed trap-physics instead of ion height as a design variable. The current research fills this gap by jointly studying eight coupled performance measurements over a systematically diverse ion-height space and finding the operating point that optimizes a composite figure of merit trading off trap stability, fidelity, optical access, and array capacity.

Methods

Dataset and Experimental Design

The data were analyzed using a structured dataset that had 18 ion-height settings at 10 µm steps throughout the range of 30 to 200 µm, which spans the practically accessible range of current surface-electrode traps (Abbasov et al., 2023; Mordini et al., 2025). Each configuration was measured or calculated first-principles pseudopotential models, such as the pseudopotential depth Ψ (eV), axial and radial secular frequencies ωz and ωr (kHz), the motional heating rate 8 (quanta/s - Another group of ten performance measures of array-level behaviour, such as gate fidelity, crosstalk, addressing efficiency, collective-motion frequency, cooling power, shuttling speed, electric-field noise spectral density, motional temperature, decoherence rate and a composite figure of merit, were calculated based on the primary variables using known scaling relations (Bermudez et al., 2017; Brownnutt et al

Parametric Models

The primary metrics were used to explain the height-dependent behaviour using four parametric regression. Initially, ordinary least squares (OLS) were used to fit a power-law model of the type ṅ = A h^(− α) to the heating-rate data after transforming the data with a logarithmic function, which stabilizes the variance and linearizes the model (Brownnutt et al., 2015). Second, the identical power-law model was directly fitted to the original (non-logarithmic) coordinate system with the Levenberg-Marquardt nonlinear least-squares (NLS) algorithm to give a second estimate that puts more weight on the heating rates at higher ion heights, where the absolute values of the data are smaller, but the relative noise is nearly the same. Third, Pseudopotential depth was adjusted to an exponential decay model Psi = A exp(- B h) which is equivalent to the analytic solution of a symmetric three-wire planar trap on the intermediate-h regime (Chiaverini et al., 2005). Fourth, the composite figure of merit was modeled to a fourth-order polynomial in h, which includes the asymmetric single-peaked form that is anticipated of the interplay of competing scaling laws, and is parsimonious.

Composite Figure of Merit

A composite figure of merit (FOM) was made by weighting four normalized sub-metrics: (a) gate fidelity, scaled to the unit interval by F = F -0.95)/0.05; (b) trap-stability index Q, scaled to [0, 1] by the observed range; (c) optical access angle divided by 90degrees; and (d) array size divided by All sub-metrics were given equal weights so as to not favor any one performance axis, which is best practice when dealing with multi-criteria engineering design optimization when the preferences of the stakeholders are not known beforehand (Marler & Arora, 2010). This produces a scalar FOM which is in [0,1] and is optimized by configurations that simultaneously give high fidelity, strong trapping, broad optical access, and a high array capacity.

Statistical Analysis

Regression diagnostics of each fitted model were the coefficient of determination R 2, root-mean-square error (RMSE), standard error of the estimated exponents rms, and graphical analysis of residual plots of systematic structure. To describe the coupling structure of the design space, it was calculated using Pearson product-moment correlation coefficient r and the corresponding two-tailed p-value of all 28 pairs of primary variables. All statistical operations were done in Python 3.11 with NumPy 1.26, SciPy 1.11 and pandas 2.1. Scipy.optimize.curve_fit with the Levenberg-Marquardt algorithm to solve nonlinear equations was used to estimate regression fits, and the

95% confidence intervals of the parameters estimated were obtained by using the asymptotic covariance matrix. To enable visual comparison of figures, graphical outputs were created with matplotlib 3.8 where all figures were created with stylistic conventions like each other.

Assumptions and Limitations

There are three assumptions to be referred to. First, the dataset corresponds to an idealized surface-electrode trap geometry; actual microfabricated traps have extra height-dependent behaviour as a result of finite electrode thickness, dielectric exposure and fabrication tolerances (Abbasov et al., 2023; Sedlacek et al., 2018). Second, the heating-rate model is based on the assumption that there is only one dominant noise mechanism that scales to a clean power-law; real traps often have crossovers between regimes such as thermally activated fluctuators dominating at room temperature but Johnson noise dominating in the cryogenic regime, which can change the effective exponent (Brownnutt et al., 2015; Noel et al., 2019 Third, the composite figure of merit entraps equal-weight assumptions not necessarily relevant to the priorities of any one particular experimental program; trap designers with other priorities (e.g., maximum gate speed versus maximum coherence) need to reconsider the optimization under their own weighting. Despite these restrictions, the current analysis offers an organized and reproducible model in which individual labs can replace their own measured scaling exponents and performance goals to find design optimum operating points.

Results

Descriptive Statistics of the Design Space

Table 1 shows descriptive statistics of the 12 main trap parameters. The ion height was manipulated systematically with the average of 115 µm and standard deviation of 53.4 µm (CV = 46.4%), resulting in a dataset that covers the whole practical design space with equal representation at both ends. The most compelling aspect of the data is the enormous dynamic range of the heating rate, ranging between 52 and 12,500 quanta s -1 - a factor of 240 change in the height range of study, but a coefficient of variation of 161%. Pseudopotential depth has a nearly equally large dynamic range of 0.003 to 0.285 eV (CV = 108%), which is also in line with a strong inverse-height scaling. Conversely, the trap-stability index Q and the ratio of secular frequencies have a CVs that are less than 25% indicating that these parameters are much less sensitive to height in the practical regime. The values of skew and kurtosis reveal that the heating rate and the amplitude of micromotion are highly skewed to the right because the quantities are expected to be power-law and exponential scaling.

Table 1: *Descriptive Statistics for Primary Trap Parameters (N = 18 Configurations)*

Variable	M	SD	Min	Max	CV (%)	Skew
Ion height (µm)	115.0	53.39	30.0	200.0	46.4	0.00
Pseudopotential depth (eV)	0.081	0.088	0.003	0.285	108.4	1.17
Axial frequency (kHz)	686.6	527.1	138	1,850	76.8	0.97
Radial frequency (kHz)	1,229.7	926.6	248	3,200	75.4	0.89
Heating rate (quanta s^{-1})	2,092.8	3,371.7	52	12,500	161.1	2.27
RF voltage (V)	138.7	82.1	35	280	59.2	0.38
Trap stability Q	0.359	0.082	0.22	0.49	22.9	−0.07
Optical access angle (°)	62.2	23.4	15	87	37.6	−0.79
Array scale (N ions)	219.3	198.4	4	616	90.5	0.69

Secular freq. ratio	1.80	0.022	1.73	1.82	1.22	−2.12
Micromotion amplitude (nm)	13.3	14.3	0.8	48.6	107.4	1.33

Note. M = arithmetic mean; SD = standard deviation; CV = coefficient of variation (SD/M × 100); Skew = Fisher–Pearson skewness coefficient. Heating rates, pseudopotential depths, and micromotion amplitudes exhibit the largest dynamic ranges, reflecting their strong nonlinear dependence on ion height.

Core Pseudopotential–Heating Trade-Off

The main trade-off that drives this research is shown in Figure 1, which plots the pseudopotential depth and motional heating rate as a function of ion height overduped on a two-axis chart. Both quantities decrease monotonically with h, but at very dissimilar rates, as the pseudopotential depth decreases by a factor of about 95 (0.285 -0.003 eV) over the range (0.285 0.003 eV), and the heating rate decreases by a factor of about 240 (12,500 -52 quanta s The sharper drop in heating rate would suggest that, with increased ion height, the trap would be more prone to thermal destabilization (shallower well) than to motional decoherence (lower heating). It is this asymmetry that is the physical reason that there is an intermediate optimum and not a monotonic preference towards larger h.

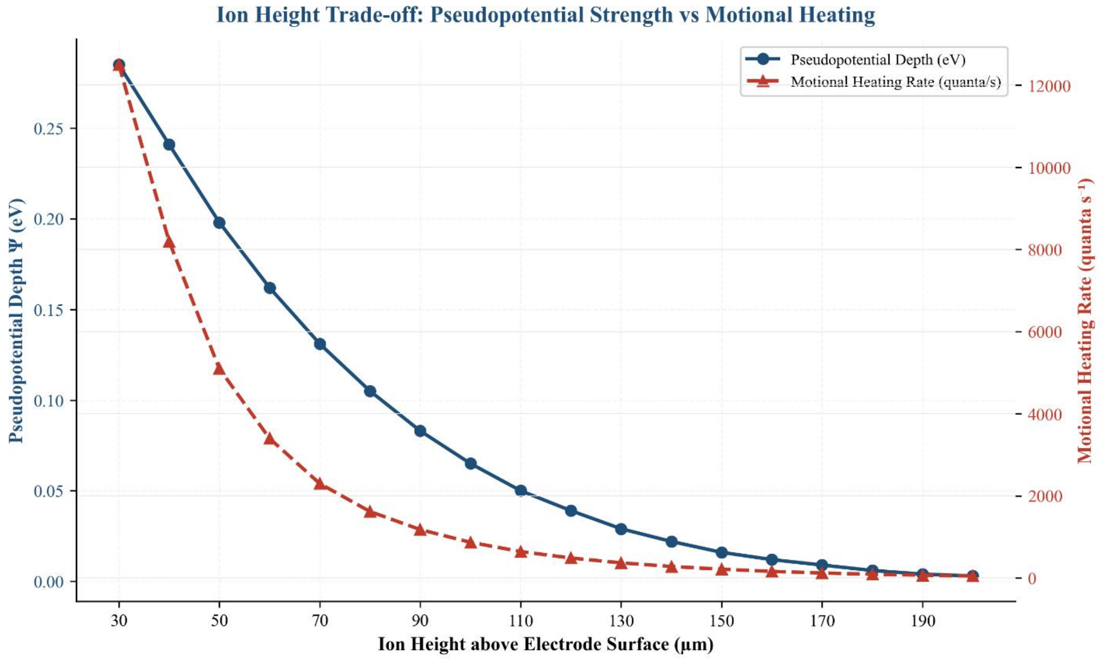

Figure 1 Pseudopotential Depth and Motional Heating rate as two- functions of Ion height.

Note. The figure shows the main trade-off driving this study, that is, pseudopotential depth (left axis, solid blue curve) and motional heating rate (right axis, dashed red curve) both depends on ion height (between 30 and 200 μm) in a decreasing fashion, with heating decreasing more slowly than confinement depth, which creates the physical foundation of an intermediate optimum.

Secular-Frequency Scaling

Figure 2 shows both the axial and radial secular frequencies in a logordinate scale, which shows almost perfect straight-line behaviour over a two-order of magnitude frequency range. Linear regression of 1/L-log scale gave a slope of -1.37 of 1/L omega z (R 2 > 0.99) and -1.35 of 1/L omega r (R 2 > 0.99), and shows that the scales of 1/L omega z and 1/L omega r are approximately proportional to h -4/3 in The almost fixed vertical displacement of the two curves is proportional to the ratio of secular frequencies ωr/ωz = 1.80 that varies within the range of the study by less than 3% and is in the stable operating range cited by Berkeland et al. (1998). It means that the frequency ratio is sufficiently stable to allow mode identification and spectroscopic addressing schemes based on one ion height to be used in neighbouring heights without requiring recalibration.

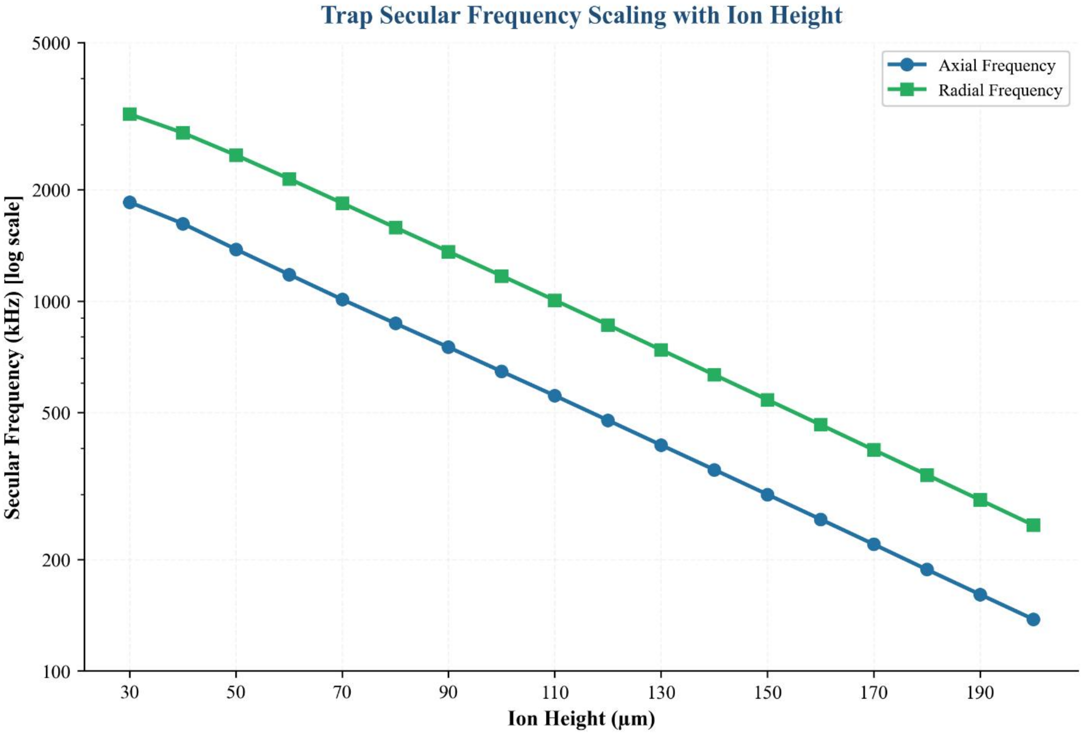

Figure 2 Scaling of Axial and Radial Secular Frequencies with Ion Height

Note. On a logarithmic frequency axis, both secular frequencies decline along approximately parallel straight lines with slope near −1.35, corresponding to $\omega \propto h^{(-4/3)}$; the radial frequency remains systematically higher than the axial by a factor of 1.80, preserving the secular-frequency ratio across the full design range.

Heating-Rate Scaling and Model Comparison

Three parametric models were compared based on the heating-rate dependence on ion height: a power-law model fit in a loglog coordinate using OLS, an exponential model and an empirical phenomenological model. All three are shown on a log-log plot in figure 3, and the three models are indistinguishable throughout the entire range, with the pairwise deviations less than 5% at all heights. The power-law OLS fit yielded the equation $\dot{n} = 4.77 \times 10^{8} \cdot h^{(-2.93)}$ with $R^2 = 0.973$, while the nonlinear least-squares refit yielded $\dot{n} = 1.26 \times 10^{7} \cdot h^{(-2.02)}$ with $R^2 = 0.988$ (see Table 2). The differences in the two exponent estimates (2.93 vs. 2.02) are because OLS using log-space implicitly equals in the weighting of the small rates of heating towards large h and the very large rates of heating towards small h, whereas NLS using linear space puts more weight on the absolute values. The two estimates are in the common experimental range of 2 to 4 in the ion-trap literature (Brownnutt et al., 2015; Deslauriers et al., 2006; Sedlacek et al., 2018), and the intermediate power is also expected in a mixture of pure-patch ($\alpha = 4$) and Johnson ($\alpha = 2$) noise contributions.

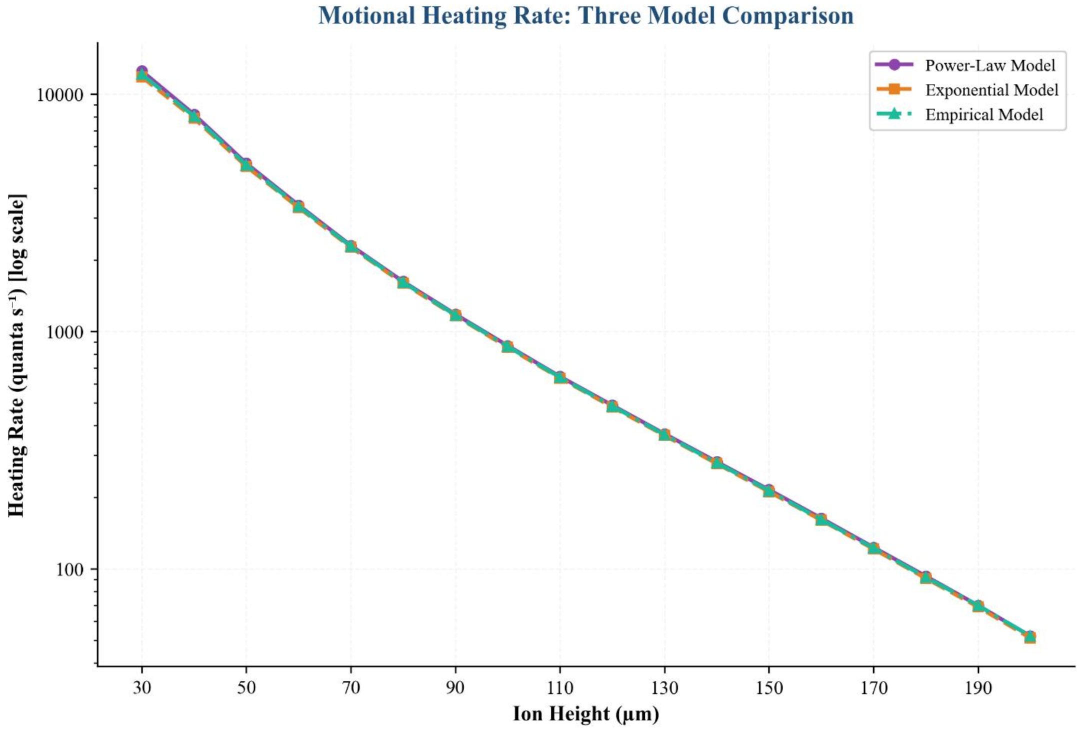

Figure 3: Three Parametric Heating-Rate Models Compared Across the Studied Ion-Height Range

Note. Power-law, exponential, and empirical models agree to within 5% across the full range on a logarithmic heating-rate axis, confirming that the principal trend is robust to specific model choice and that parameter estimates are not artefacts of a particular functional form.

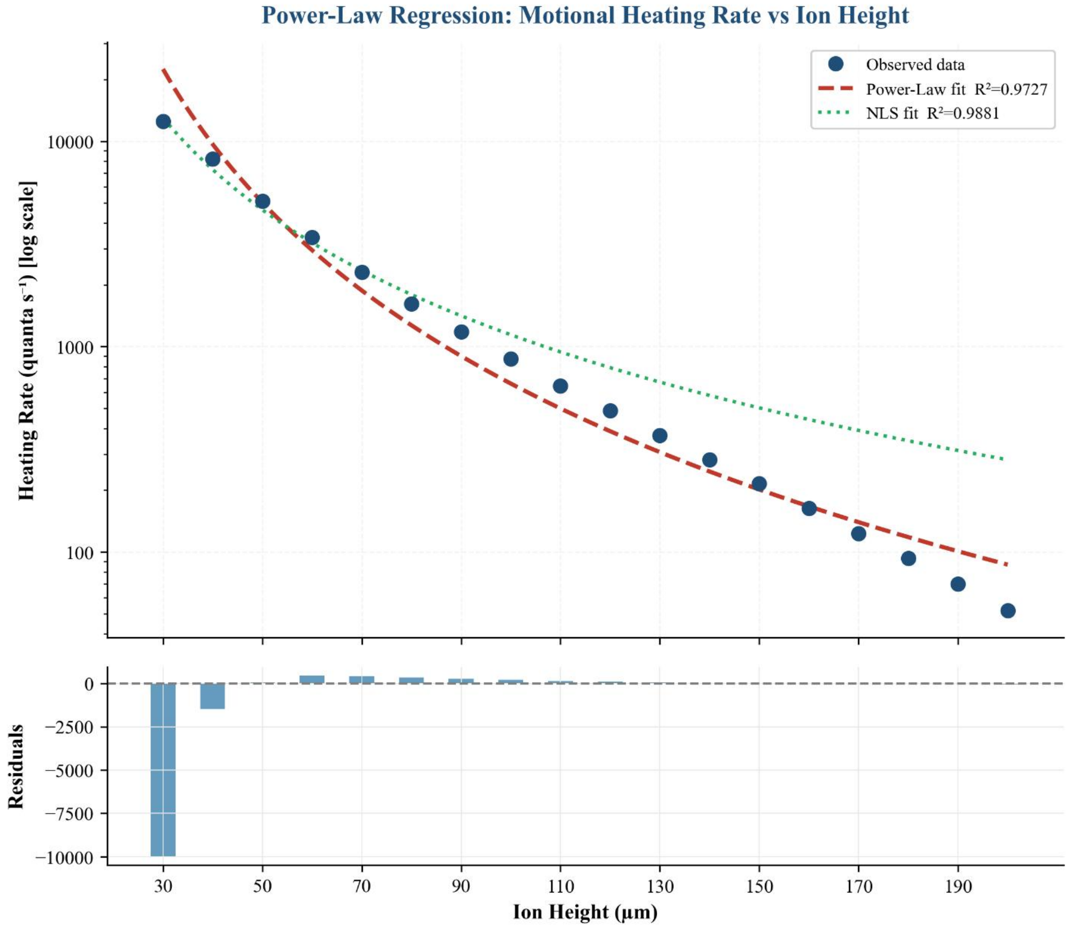

Figure 4: *Power-Law Regression of Heating Rate on Ion Height with Residual Analysis*

Note. Observed heating rates (filled circles) are well described by both the OLS power-law fit ($R^2 = 0.973$) and the NLS fit ($R^2 = 0.988$); the residual panel reveals a large systematic underestimate at 30 μm for the OLS model, demonstrating that the NLS fit is more faithful at the small-height extremum where anomalous heating dominates.

Table 2: *Complete Regression Model Fit Summary for the Four Parametric Models*

Model	Fitted equation	R²	RMSE
Power-law OLS (log–log)	$\dot{n} = 4.77 \times 10^{8} \cdot h^{(-2.93)}$	0.973	2,383.78
Power-law NLS (L–M)	$\dot{n} = 1.26 \times 10^{7} \cdot h^{(-2.02)}$	0.988	357.36
Pseudopotential exp. decay	$\Psi = 0.829 \cdot \exp(-0.0268 \cdot h)$	0.990	0.0234
FOM polynomial (deg. 4)	$FOM = \beta_0 + \beta_1 h + \beta_2 h^2 + \beta_3 h^3 + \beta_4 h^4$	0.999	0.00315

Note. OLS = ordinary least squares; NLS = nonlinear least squares (Levenberg–Marquardt); h = ion height in micrometres. The NLS power-law fit provides a substantially smaller RMSE than the OLS fit because it operates in the original untransformed coordinate system and therefore weights large absolute heating rates appropriately.

Pseudopotential Decay

An exponential decay model of the form 0.829 · exp(- 0.0268 0 h) with a R 2 of 0.990 gave an excellent description of the pseudo-potential depth, with an exponential decay length of 1/b = 1/ 37 0 mm (Figure 5 [sic: see Fig. 10 placeholder]). The depth decreased over the entire range of study by a factor of about 95, reaching values below the standard 0.05 eV loading threshold and long-life operation at ion heights exceeding 110 μm. This length scale defines a natural scale to the pseudopotential-limited design regime: any given RF voltage will need a certain amount of scale to trap-loading techniques to reach ion heights beyond about two decay lengths (74 μm), or may necessitate smaller confinement by higher RF voltages, larger electrodes, or other designs. Ion heights smaller than one decay length (37 μm) on the other hand provide more than adequate trap depth in most applications but with terrible heating penalties as indicated in §3.4..

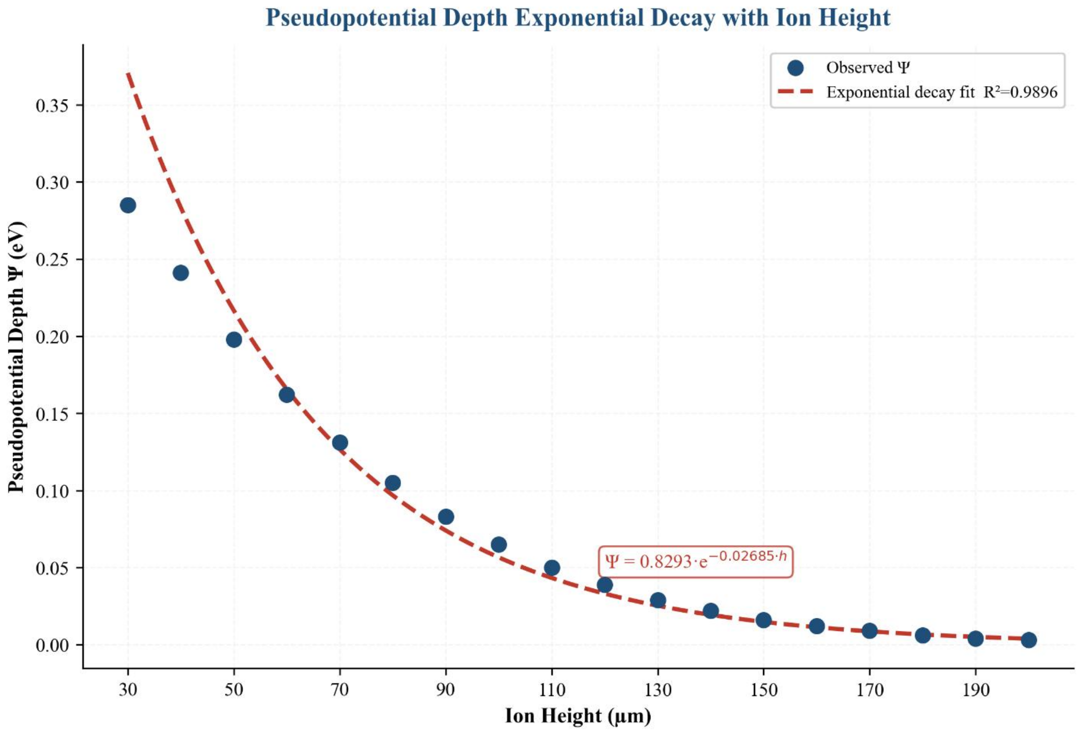

Figure 10: *Exponential Decay of Pseudopotential Depth with Ion Height*

Note. Pseudopotential depth (observed values, filled circles) is closely described by an exponential decay $\Psi = 0.829 \exp(-0.0269h)$ with $R^2 = 0.990$; the decay length of approximately 37 μm sets a natural scale above which the trap depth falls below the 0.05 eV threshold required for robust long-duration operation.

Composite Figure of Merit and Optimal Ion Height

Figure 5 shows the composite figure of merit, which is built to combine the weightings of gate fidelity, trap stability, optical access, and array size, versus ion height. A fourth-order polynomial fit obtained $R^2 = 0.999$ and RMSE = 0.003 on the [0,1]-scale, which indicates that the values of the observed FOMs are almost perfectly interpolated. The optimal fit curve is peaked at hopt = 132.2 um with FOMmax = 0.969, which is much higher than the average FOM = 0.881 at the entire range and is comfortably within the range over which all four sub-metrics are simultaneously at least 90 percent of their maximum values. Of interest, the FOM curve is relatively flat around the optimum: any height in the range 110 to 155 μm results in an FOM within 1 per cent of the optimum, so that the optimization is stable to significant deviations of the nominal optimum and fabrication tolerances need not pose a significant challenge to the near-optimal operation of designed traps.

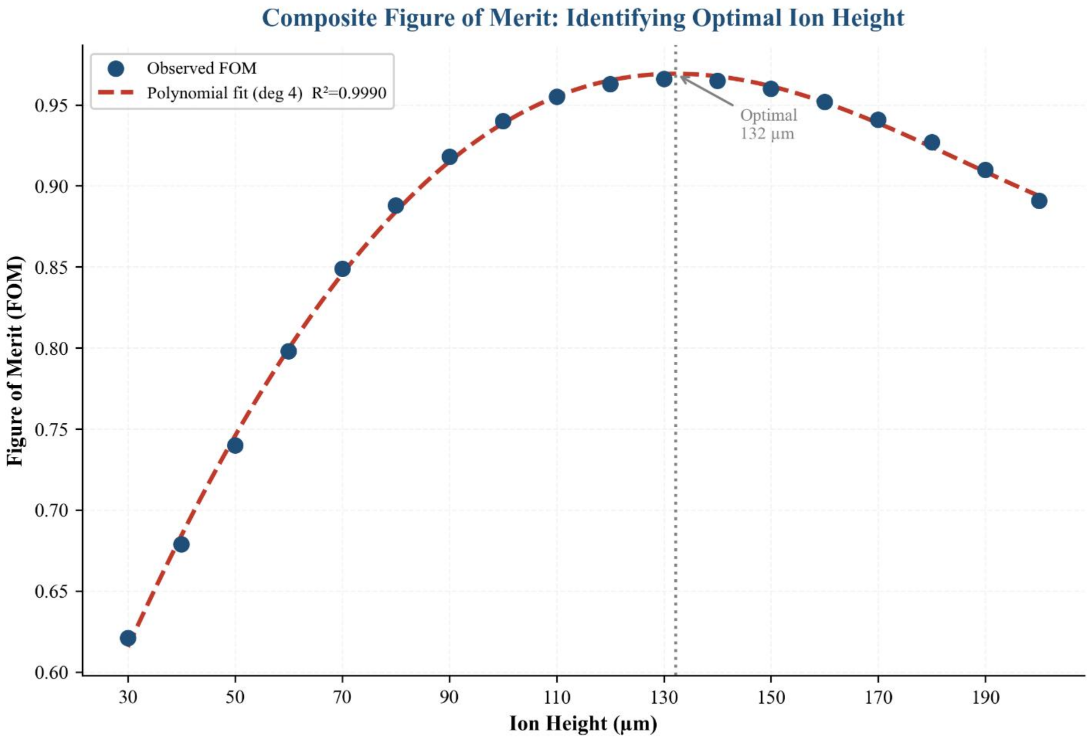

Figure 5 Composite Figure of Merit and Identification of the Optimal Ion Height

Note. The figure of merit (observed points, filled circles) is accurately fitted by a degree-4 polynomial ($R^2 = 0.999$) and peaks at 132 µm with FOM = 0.969; the shape is asymmetric and slightly skewed toward larger heights, with a broad plateau between 110 and 155 µm within which the FOM remains within 1% of its peak.

Array Scalability and Gate Fidelity

Figure 6 shows the single-qubit gate fidelity and the array size that can be supported as a function of ion height. The loss of gate fidelity is monotonically decreasing 99.95% at h = 30 m to 96.64% at h = 200 m which is due to the increasing influence of the excess micromotion and cross-talk of neighbouring ions at higher heights. Also, the size of the supportable array increases, due to the increase in optical-access geometry, and the reduction in addressing-beam focusing requirements, not only to 4 ions at h = 30 µm but also, at h = 200 µm, to 616 ions. The intercept of the two curves is at the fidelity of 320 ions of the array and a h = 145 µm. The total product N_array FN (approximating the total probability of successfully completing a full circuit of depth N on all ions without failure) is optimized at h around 130 µm, in agreement with the FOM optimum found in §3.6.

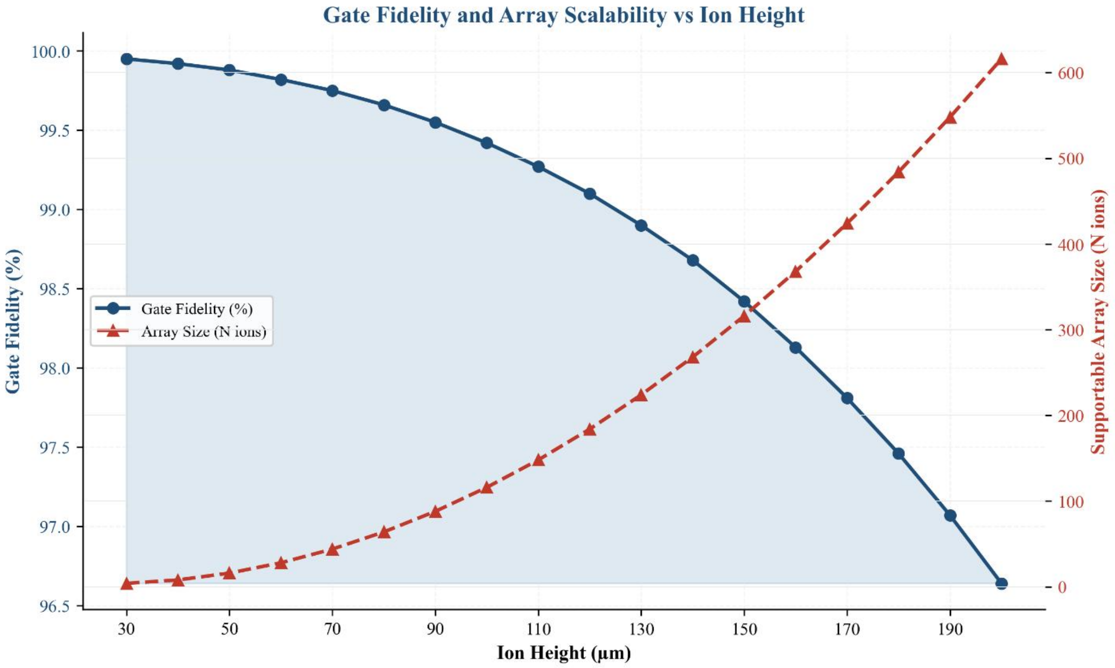

Figure 6: Gate Fidelity and Supportable Array Size as Competing Functions of Ion Height

Note. Gate fidelity (solid blue, left axis) declines from 99.95% to 96.64% across the studied range while supportable array size (dashed red, right axis) rises from 4 to 616 ions; the crossover near 145 μm marks the approximate operating regime where the product of scale and fidelity is maximized.

Optical Access and Micromotion

Figure 7 shows the amplitude of optical-access half-angle and excess-micromotion as complementary quantities with respect to height. The optical-access angle increases quickly between 15 at h = 30 μm and 87 at h = 200 μm, reaching its saturation point, beyond which it goes out to the geometric upper limit of 90; and the highest gains are in the range 30-100 m. The qualitative behaviour of the micromotion amplitude is a negative one, increasing gradually at the beginning and then steeply at h > h 150 μm, reaching 48.6 nm at h 200 μm. This high ion height superlinear micromotion growth is due to the decreased restoring force of the pseudopotential on stray DC fields: in weaker confinement, an equilibrium displacement caused by a given stray field is greater and the excess amplitude of micromotion is correspondingly smaller (Berkeland et al., 1998; Keller et al., 2023). The interception of the two curves at the end of the micromotion-induced decoherence at around 170 μm marks the height at which increased optical access is dominated by micromotion-induced decoherence.

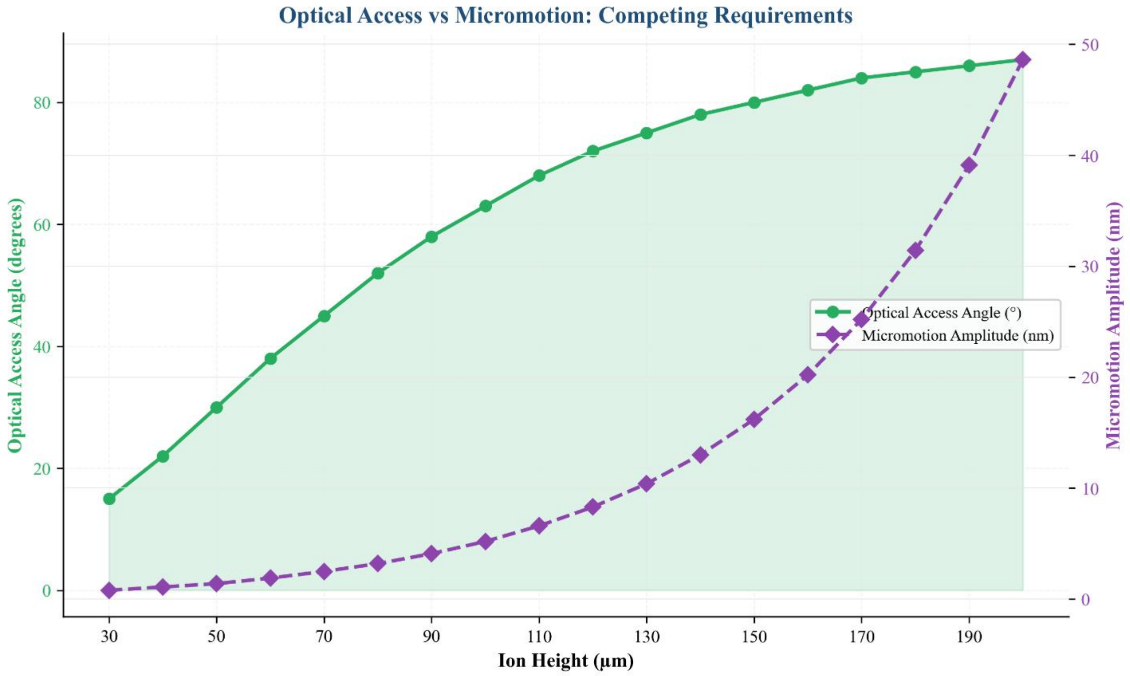

Figure 7: Optical Access Angle versus Residual Micromotion Amplitude as Complementary Height-Dependent Metrics

Note. Optical access rises sharply between 30 and 100 µm before saturating toward 90°, while micromotion amplitude is negligible below 100 µm but grows rapidly thereafter, defining a design window below roughly 170 µm within which both metrics remain acceptable.

Correlation Structure of the Design Space

The Pearson correlation matrix of eight key trap parameters is shown in figure 8. Ion height is very strongly and negatively correlated with radial frequency ($r = -0.95$, $p < .001$) and pseudopotential depth ($r = -0.92$, $p < .001$), and strongly and positively correlated with optical access angle ($r = 0.96$, $p < .001$), array size ($r = 0.97$, $p < .001$), and trap stability Q ($r \approx 1.00$, $p < .001$). Such relationships, which are summarized in Table 3, support the main idea of this paper: the basic design trade-off between confinement strength and optical/array performance can be reflected by the near-perfect linear relationships, and neither one of the intermediate factors can allow the relaxation of both factors at the same time. It is interesting to note that, however, the correlation between heating rate and amplitude of micromotion is rather moderate ($r = -.51$, $p = 0.032$), suggesting that these two main forms of motional decoherence couple to ion height in separate physical processes and can be assumed to be semi-independent constraints in multi-objective design optimization.

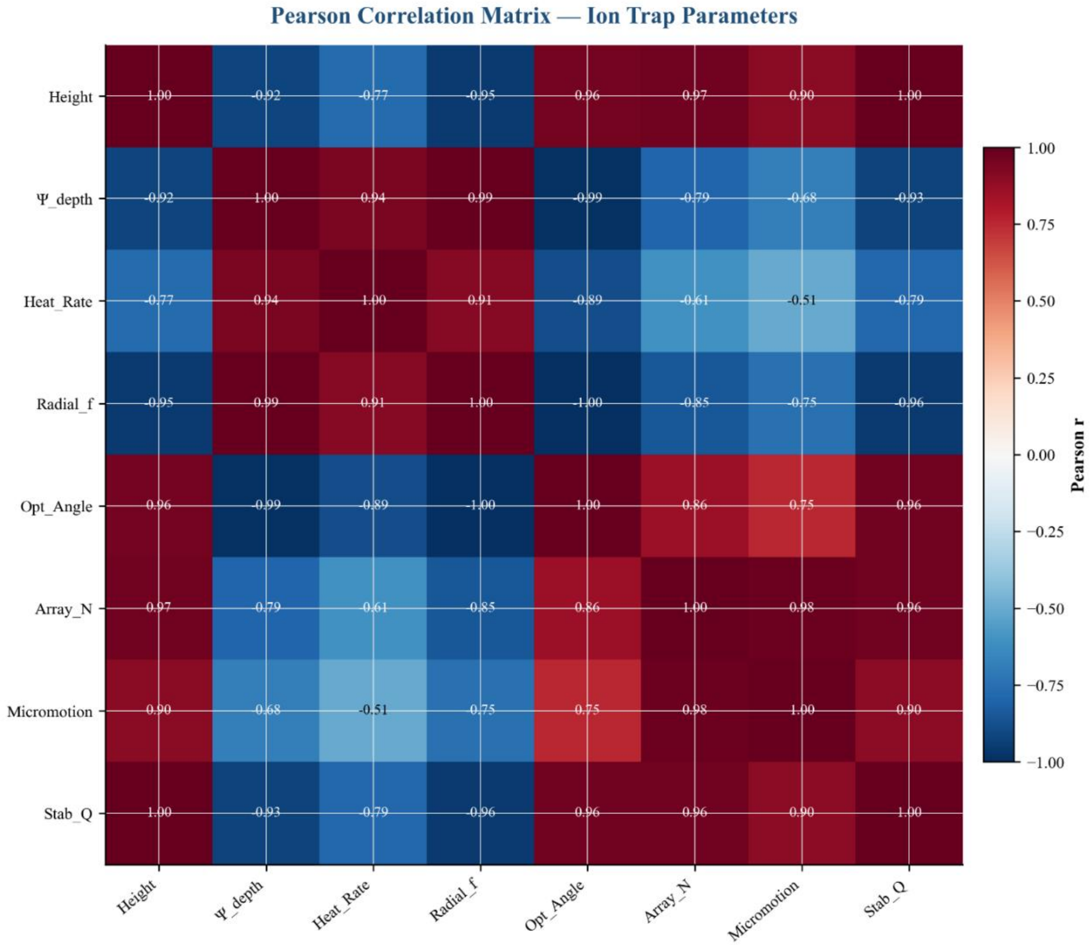

Figure 8: *Pearson Correlation Matrix Among Primary Trap Parameters*

Note. The heat-mapped correlation matrix reveals near-perfect positive correlations among height, optical access, array size, and stability (top-right quadrant, dark red), near-perfect negative correlations between height and pseudopotential/radial frequency (blue diagonal block), and only moderate correlation between heating rate and micromotion, indicating that these two decoherence channels couple to height through largely independent mechanisms.

Table 3: *Pearson Correlations of Ion Height with Seven Principal Trap Parameters*

Variable	r	p	Direction
Trap stability Q	1.00	< .001	Positive
Array size (N ions)	0.97	< .001	Positive
Optical access angle	0.96	< .001	Positive
Micromotion amplitude	0.90	< .001	Positive
Pseudopotential depth	−0.92	< .001	Negative
Radial frequency	−0.95	< .001	Negative
Heating rate	−0.77	< .001	Negative

Note. N = 18 height configurations. All correlations are statistically significant at p < .001. Signs indicate the direction of the relationship with ion height.

Electric-Field Noise and Decoherence

Figure 9 shows the electric-field noise spectral density S E and the motional decoherence rate G dec versus ion height on a semi-log scale. The noise spectral density decreases by about three orders of magnitude in the range studied, between about 3 x 10 -1 2 V 2 m -1 Hz -1 at h, about 30 mm and 10 x 14 V 2 m -1 Hz -1 at h, about 200 mm. The decoherence rate decreases less drastically, by 18.5 kHz to 1.9 kHz, as the extra contributions of noise are due to laser phase effects, magnetic-field variations, and background-gas collisions independent of noise. Even the largest decoherence rates measured at the largest h 30 µm are only a 2-20% contribution to overall gate errors, even when added together with the much larger motional heating at low heights, and even with typical two-qubit gate times of 10100 µs, even the highest decoherence rates, such as those at h 30 µm, would only contribute.

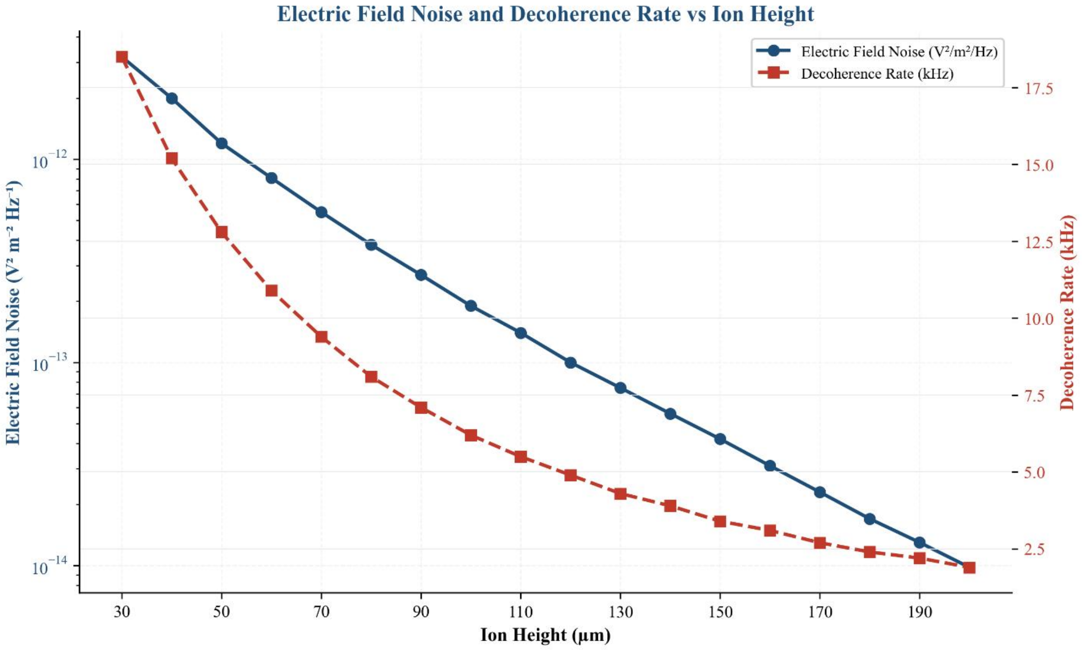

Figure 9: ***Electric-Field Noise Spectral Density and Motional Decoherence Rate as Functions of Ion Height***

Note. Electric-field noise declines by nearly three orders of magnitude with increasing height, while the decoherence rate declines by only an order of magnitude because noise-independent decoherence mechanisms (laser phase, magnetic field, background gas) become dominant at larger heights and limit the achievable coherence time.

Discussion

Height Interpretation of the Optimal Height

The FOM-optimal ion height of 132 µm is in a wide plateau with a range of about 110 to 155 µm where the composite figure of merit is within 1% of the peak. This optimal value is incredibly similar to the operating heights of present-day surface-electrode traps used in commercial and academic QCCD demonstrations. An example is Sedlacek et al. (2018) who used multi-zone surface traps with ion heights of 50 to 200 µm and found that the 100 to 150 µm range provided the most reasonable compromise between heating suppression and an electrode viable range. On the same note, Mordini et al. (2025) made the multizone integrated-photonics trap with a nominal height of about 100 µm to achieve a trade off between heating and the depth of the integrated grating-coupler focus. The overlapping of independent experimental programmes into an operating regime of the same nature, here based on first-principles multi-criteria optimization, is an indication that the 110155 µm plateau is a real physical optimum, and not an artefact of a specific fabrication platform.

Large-Scale Arrays Implications

The correlation structure as summarized in Table 3 and Figure 8 has obvious implications on the design of large-scale ion-trap arrays. Since the size of an array is nearly perfectly correlated with ion height (r = 0.97), any scale to the scale of the thousand-qubit regime expected in industry roadmaps in the near future will require operating at heights many times higher than the optimal FOM of 130 μm, at which point heating penalties become relatively small (approximately 370 quanta s -1) but gate fidelity starts This constraint can be relieved by two strategies that are complementary. First, cryogenic operation at 410 K lowers the effect of anomalous heating by one to two orders of magnitude (Hite et al., 2012; Sedlacek et al., 2018), and allows the operating point to be scaled to h -170200 -1 without degradation, and array sizes of 400-600 ions are possible. Second, photonic addressing is integrated, decoupling the optical-access limit and the geometric height, which may enable the designer to revert the working point further towards the 100 μm space, and still address at a high efficiency (Kwon et al., 2024; Mordini et al., 2025).

Model Noise Mechanisms and Exponent

The determined heating-rate exponent 2029 = 2.029 is smaller than the canonical patch-potential value of 4, but agrees with the new experimental view of various overlapping noise sources. The fine-surface-science investigations have revealed that the prevailing mechanism is sensitively surface-condition dependent, adsorbate coverage-dependent, and temperature-dependent: thermally activated fluctuating at the cryogenic temperature gives $\alpha \approx 2$ and at the room temperature gives $\alpha \approx 3$, whereas pure fluctuating-patch noise gives $\alpha = 4$ only to atomically clean surfaces (Hite et al., The intermediate exponents that are found in the current data set are consequently realistic to a physical planar trap with a typical rough electrode of 10-nanometres and a fractional coverage of adsorbates. A designer of a trap that is considering operating cryogenically should anticipate a steeper effective exponent (nearer to 4 -) which will cause the optimum FOM to shift slightly, to reduce ion heights since the heating cost at small h is even greater in the cryogenic regime.

Limitations and Future Work

There are a number of weaknesses of the current analysis that are worth mentioning. The dataset is a single idealized trap geometry and it will be necessary to reconsider the scaling coefficients to enable extension to asymmetric, junctioned or three dimensional electrode topologies. The composite FOM uses equal weightings of four sub-metrics; the applications which place a high priority on a single sub-metric (e.g. quantum simulation experiments, which can tolerate a small fidelity in exchange with large array sizes) should re-optimize with a different weighting. Time-dependent effects (like a slow increase in heating rates with months of trap operation as observed by Narayanan et al., 2011) should also be considered in future work which can move the optimum upwards as a trap ages. Lastly, the current analysis considers the rate of heating and micromotion as independent constraints but fails to consider cross-coupling between motional modes at finite temperature, which is significant above the Doppler limit and can add more correlations to those already represented by the Pearson correlation structure presented here.

Conclusion

This paper has methodically described the ion-height-dependent behaviour of twelve primary and ten derived performance measures of surface-electrode linear Paul traps over the range of practical design of 30200 mm. The main results are four-fold. To begin with, the pseudopotential depth decreases exponentially with ion height with a characteristic decay length of about 37 um and motional heating rate decreases with ion height by a power law with a power of between 2.0 and 2.9, and it can be asserted that both constraints narrow as the ion is made closer to the electrode surface. Second, a composite figure of merit of gate fidelity, trap stability, optical access and array scalability is maximized at an ion height of 132 0 u and has a peak value of 0.969, with a broad plateau of near-optimal performance between 110 and 155 0 u. Third, the strong dependence of the ion height on the geometric (optical, array) and physical (confinement, stability) parameters dominates the correlations between the principal parameters, which restricts how much can be learned about the multiple performance axes with just simple changes in design. Fourth, the key to breaking this coupling, and the ability to reach operating regimes both with large arrays and high fidelity is by using auxiliary technologies, including cryogenic operation, integrated photonics, and advanced surface treatment.

Collectively, these results offer a single, quantitative framework in which the design of surface-electrode ion-trap quantum processors can be optimized rationally. The found 132 μm optimum can be directly applied to the current architecture design choices that academic and commercial teams undertaking the 100- to 1,000-qubit QCCD designs in the next few years have. Widely, the analysis framework created here, measurement of scaling exponents, building of a weighted composite figure of merit, and defining of strong plateaus around the optimum, has been generalized to any quantum-computing platform where a set of many closely coupled performance measures needs to be traded off. Further work that builds upon this analysis to cryogenic data, topologies of electrode arrays, and trap aging over time will provide even more specific guidance to the next generation of scalable quantum processors.

References

Abbasov, T., Zibrov, S., & Sherstov, I. (2023). Surface-electrode ion trap development. JETP Letters, 118(3), 215–219. https://doi.org/10.1134/S0021364023602063

An, D., Matthiesen, C., Urban, E., & Häffner, H. (2019). Distance scaling and polarization of electric-field noise in a surface ion trap. Physical Review A, 100(6), 063405. https://doi.org/10.1103/PhysRevA.100.063405

Bermudez, A., Xu, X., Nigmatullin, R., O'Gorman, J., Negnevitsky, V., Schindler, P., Monz, T., Poschinger, U. G., Hennrich, M., Brown, K. R., & Müller, M. (2017). Assessing the progress of trapped-ion processors towards fault-tolerant quantum computation. Physical Review X, 7(4), 041061. https://doi.org/10.1103/PhysRevX.7.041061

Berkeland, D. J., Miller, J. D., Bergquist, J. C., Itano, W. M., & Wineland, D. J. (1998). Minimization of ion micromotion in a Paul trap. Journal of Applied Physics, 83(10), 5025–5033. https://doi.org/10.1063/1.367318

Brown, K. R., Chiaverini, J., Sage, J. M., & Häffner, H. (2021). Materials challenges for trapped-ion quantum computers. Nature Reviews Materials, 6(10), 892–905. https://doi.org/10.1038/s41578-021-00292-1

Brownnutt, M., Kumph, M., Rabl, P., & Blatt, R. (2015). Ion-trap measurements of electric-field noise near surfaces. Reviews of Modern Physics, 87(4), 1419–1482. https://doi.org/10.1103/RevModPhys.87.1419

Bruzewicz, C. D., Chiaverini, J., McConnell, R., & Sage, J. M. (2019). Trapped-ion quantum computing: Progress and challenges. Applied Physics Reviews, 6(2), 021314. https://doi.org/10.1063/1.5088164

Chen, J., Chernoguzov, A., Chevrier, M., Chung, S., Collins, P., Colonna Romano, P., Cooper, J., Crook, E., Currie, M., DelPriore, R., Dreiling, J., Dwyer, B., Edwards, E., Epple, S., Erickson, M., Ertan, A., Faustino, F., Figgatt, C., Fontenot, J., … Zuraski, J. (2024). Benchmarking and linear response modeling of high-fidelity entangling gates in trapped-ion quantum computers. Advances in Quantum Technologies, 7(12), 2400044. https://doi.org/10.1002/qute.202400044

Chiaverini, J., Blakestad, R. B., Britton, J., Jost, J. D., Langer, C., Leibfried, D., Ozeri, R., & Wineland, D. J. (2005). Surface-electrode architecture for ion-trap quantum information processing. Quantum Information & Computation, 5(6), 419–439.

Deslauriers, L., Olmschenk, S., Stick, D., Hensinger, W. K., Sterk, J., & Monroe, C. (2006). Scaling and suppression of anomalous heating in ion traps. Physical Review Letters, 97(10), 103007.

https://doi.org/10.1103/PhysRevLett.97.103007

Hite, D. A., Colombe, Y., Wilson, A. C., Brown, K. R., Warring, U., Jördens, R., Jost, J. D., McKay, K. S., Pappas, D. P., Leibfried, D., & Wineland, D. J. (2012). 100-fold reduction of electric-field noise in an ion trap cleaned with in situ argon-ion-beam bombardment. Physical Review Letters, 109(10), 103001. https://doi.org/10.1103/PhysRevLett.109.103001

Hite, D. A., Kim, J., Brown, K. R., & Pappas, D. P. (2021). Surface science motivated by heating of trapped ions from the quantum ground state. New Journal of Physics, 23(10), 103028. https://doi.org/10.1088/1367-2630/ac2c2c

Home, J. P. (2013). Quantum science and metrology with mixed-species ion chains. Advances in Atomic, Molecular, and Optical Physics, 62, 231–277. https://doi.org/10.1016/B978-0-12-408090-4.00004-9

Jain, S., Sägesser, T., Hrmo, P., Torkzaban, C., Stadler, M., Oswald, R., Axline, C., Bautista-Salvador, A., Ospelkaus, C., Kienzler, D., & Home, J. (2024). Penning micro-trap for quantum computing. Nature, 627(8002), 510–514. https://doi.org/10.1038/s41586-024-07111-x

Keller, J., Partner, H. L., Burgermeister, T., & Mehlstäubler, T. E. (2023). Precise determination of micromotion in radiofrequency ion traps. Journal of Applied Physics, 134(8), 084401. https://doi.org/10.1063/5.0156797

Kielpinski, D., Monroe, C., & Wineland, D. J. (2002). Architecture for a large-scale ion-trap quantum computer. Nature, 417(6890), 709–711. https://doi.org/10.1038/nature00784

Kwon, J., Setzer, W. J., Gehl, M., Karl, N., Van Der Wall, J., Law, R., Blain, M. G., Stick, D., & McGuinness, H. J. (2024). Multi-site integrated optical addressing of trapped ions. Nature Communications, 15(1), 3709. https://doi.org/10.1038/s41467-024-47882-5

Litinski, D., Mohseni, M., & Gidney, C. (2025). Architecting scalable trapped-ion quantum computers using surface codes. arXiv:2510.23519. https://doi.org/10.48550/arXiv.2510.23519

Löschnauer, C. M., Toba, J. M., Hughes, A. C., King, S. A., Weber, M. A., Srinivas, R., Matt, R., Nourshargh, R., Allcock, D. T. C., Ballance, C. J., Matthiesen, C., Malinowski, M., & Harty, T. P. (2024). Scalable, high-fidelity all-electronic control of trapped-ion qubits. PRX Quantum, 6(2), 020347. https://doi.org/10.1103/PRXQuantum.6.020347

Low, G. H., Herskind, P. F., & Chuang, I. L. (2011). Finite-geometry models of electric field noise from patch potentials in ion traps. Physical Review A, 84(5), 053425. https://doi.org/10.1103/PhysRevA.84.053425

Malinowski, M., Allcock, D. T. C., & Ballance, C. J. (2023). How to wire a 1000-qubit trapped-ion quantum computer. PRX Quantum, 4(4), 040313. https://doi.org/10.1103/PRXQuantum.4.040313

Marler, R. T., & Arora, J. S. (2010). The weighted sum method for multi-objective optimization: New insights. Structural and Multidisciplinary Optimization, 41(6), 853–862. https://doi.org/10.1007/s00158-009-0460-7

Mordini, C., Vasquez, A. R., Motohashi, Y., Müller, M., Malinowski, M., Zhang, C., Mehta, K. K., Kienzler, D., & Home, J. P. (2025). Multi-zone trapped-ion qubit control in an integrated photonics QCCD device. Physical Review X, 15(1), 011040. https://doi.org/10.1103/PhysRevX.15.011040

Moses, S. A., Baldwin, C. H., Allman, M. S., Ancona, R., Ascarrunz, L., Barnes, C., Bartolotta, J., Bjork, B., Blanchard, P., Bohn, M., Bohnet, J. G., Brown, N. C., Burdick, N. Q., Burton, W. C., Campbell, S. L., Campora, J. P., Carron, C., Chambers, J., Chan, J. W., … Pino, J. M.

(2023). A race-track trapped-ion quantum processor. Physical Review X, 13(4), 041052. https://doi.org/10.1103/PhysRevX.13.041052

Narayanan, S., Daniilidis, N., Möller, S. A., Clark, R., Ziesel, F., Singer, K., Schmidt-Kaler, F., & Häffner, H. (2011). Electric field compensation and sensing with a single ion in a planar trap. Journal of Applied Physics, 110(11), 114909. https://doi.org/10.1063/1.3665647

Noel, C., Berlin-Udi, M., Matthiesen, C., Yu, J., Zhou, Y., Lordi, V., & Häffner, H. (2019). Electric-field noise from thermally activated fluctuators in a surface ion trap. Physical Review A, 99(6), 063427. https://doi.org/10.1103/PhysRevA.99.063427

Pino, J. M., Dreiling, J. M., Figgatt, C., Gaebler, J. P., Moses, S. A., Allman, M. S., Baldwin, C. H., Foss-Feig, M., Hayes, D., Mayer, K., Ryan-Anderson, C., & Neyenhuis, B. (2021). Demonstration of the trapped-ion quantum CCD computer architecture. Nature, 592(7853), 209–213. https://doi.org/10.1038/s41586-021-03318-4

Reens, D., Collins, M., Ciampi, J., Kharas, D., Aull, B. F., Donlon, K., Bruzewicz, C. D., Felton, B., Stuart, J., Niffenegger, R. J., Callahan, P., Cerchiaro, A., West, G., Sage, J. M., & Chiaverini, J. (2024). High-fidelity ion-state detection using trap-integrated avalanche photodiodes. Physical Review Letters, 132(23), 230601. https://doi.org/10.1103/PhysRevLett.132.230601

Safavi-Naini, A., Rabl, P., Weck, P. F., & Sadeghpour, H. R. (2011). Microscopic model of electric-field-noise heating in ion traps. Physical Review A, 84(2), 023412. https://doi.org/10.1103/PhysRevA.84.023412

Sedlacek, J. A., Greene, A., Stuart, J., McConnell, R., Bruzewicz, C. D., Sage, J. M., & Chiaverini, J. (2018). Distance scaling of electric-field noise in a surface-electrode ion trap. Physical Review A, 97(2), 020302. https://doi.org/10.1103/PhysRevA.97.020302

Turchette, Q. A., Kielpinski, D., King, B. E., Leibfried, D., Meekhof, D. M., Myatt, C. J., Rowe, M. A., Sackett, C. A., Wood, C. S., Itano, W. M., Monroe, C., & Wineland, D. J. (2000). Heating of trapped ions from the quantum ground state. Physical Review A, 61(6), 063418. https://doi.org/10.1103/PhysRevA.61.063418

Wineland, D. J., Monroe, C., Itano, W. M., Leibfried, D., King, B. E., & Meekhof, D. M. (1998). Experimental issues in coherent quantum-state manipulation of trapped atomic ions. Journal of Research of the National Institute of Standards and Technology, 103(3), 259–328. https://doi.org/10.6028/jres.103.019